

Hydrogen bond residue positioning in the 599–611 loop of thimet oligopeptidase is required for substrate selection

Lisa A. Bruce¹, Jeffrey A. Sigman², Danica Randall², Scott Rodriguez², Michelle M. Song¹, Yi Dai¹, Donald E. Elmore¹, Amanda Pabon³, Marc J. Glucksman³ and Adele J. Wolfson¹

¹ Chemistry Department, Wellesley College, MA, USA

² Chemistry Department, Saint Mary's College of California, Moraga, CA, USA

³ Midwest Proteome Center and Department of Biochemistry and Molecular Biology, Rosalind Franklin University of Medicine and Science, Chicago, IL, USA

Keywords

enzyme flexibility; hydrogen bonding; metallopeptidase; substrate selectivity; thimet oligopeptidase

Correspondence

A. J. Wolfson, Wellesley College, Office of the Dean of the College, 106 Central Street, Wellesley, MA 02481-8203, USA
 Fax: 1 781 283 3695
 Tel: 1 781 283 3583
 E-mail: awolfson@wellesley.edu

(Received 28 July 2008, revised 15 September 2008, accepted 17 September 2008)

doi:10.1111/j.1742-4658.2008.06685.x

Thimet oligopeptidase (EC 3.4.24.15) is a zinc(II) endopeptidase implicated in the processing of numerous physiological peptides. Although its role in selecting and processing peptides is not fully understood, it is believed that flexible loop regions lining the substrate-binding site allow the enzyme to conform to substrates of varying structure. This study describes mutant forms of thimet oligopeptidase in which Gly or Tyr residues in the 599–611 loop region were replaced, individually and in combination, to elucidate the mechanism of substrate selection by this enzyme. Decreases in k_{cat} observed on mutation of Tyr605 and Tyr612 demonstrate that these residues contribute to the efficient cleavage of most substrates. Modeling studies showing that a hinge-bend movement brings both Tyr612 and Tyr605 within hydrogen bond distance of the cleaved peptide bond supports this role. Thus, molecular modeling studies support a key role in transition state stabilization of this enzyme by Tyr605. Interestingly, kinetic parameters show that a bradykinin derivative is processed distinctly from the other substrates tested, suggesting that an alternative catalytic mechanism may be employed for this particular substrate. The data demonstrate that neither Tyr605 nor Tyr612 is necessary for the hydrolysis of this substrate. Relative to other substrates, the bradykinin derivative is also unaffected by Gly mutations in the loop. This distinction suggests that the role of Gly residues in the loop is to properly orientate these Tyr residues in order to accommodate varying substrate structures. This also opens up the possibility that certain substrates may be cleaved by an open form of the enzyme.

Thimet oligopeptidase (TOP, EC 3.4.24.15), a 78 kDa, zinc-dependent endopeptidase, contains the HEXXH sequence in its active site, common to other endopeptidases of the M3 family of metallopeptidases [1–3]. This zinc-binding motif causes the attack of an activated water molecule at the carbonyl carbon of the scissile peptide bond and the formation of a tetra-

hedral oxyanion intermediate [4]. TOP is most closely related to neurolysin (EC 3.4.24.16), with which it shares 60% sequence identity, overall three-dimensional structure, and the ability to target and hydrolyze numerous short peptides (< 17 residues) involved in various physiological processes [3,5–7]. Consistent with TOP's broad anatomic and subcellular distribution, it

Abbreviations

DcP, bacterial dipeptidyl carboxypeptidase from *Escherichia coli*; Dnp, 2,4-dinitrophenol; MCA, 7-methoxycoumarin-4-acetyl-Pro-Leu-Gly-Pro-Lys-dinitrophenol; mcaBk, 7-methoxycoumarin-4-acetyl-[Ala⁷, Lys(dinitrophenol)⁹]-bradykinin; mca, methoxycoumarin; mcaGnRH_{1–9}, mca-Glu-His-Trp-Ser-Tyr-Gly-Leu-Arg-Pro-OH; mcaNt, mca-Leu-Glu-Asn-Lys-Pro-Arg-Arg-Pro-Lys(Dnp)-OH; TCEP, tris(2-carboxyethyl)phosphine hydrochloride; TOP, thimet oligopeptidase.

is implicated in the hydrolysis of peptide substrates involved in vital functions, such as blood pressure control, reproduction, nociception and antigen presentation [8–13].

A distinguishing feature of the X-ray crystallographically derived structures of the apo- (substrate free) forms of TOP [14] and neurolysin [4] is their catalytic site, located in a deep channel that limits the size and shape of accessible substrates [14]. At the base of the channel are conserved flexible loop regions that contribute to the specificity of these two enzymes. One particular loop in neurolysin, composed of residues 600–612 and located across from the enzyme's active site, appears to be highly mobile because it includes five Gly residues [4,14,15]. TOP's corresponding loop, residues 599–611, contains one fewer Gly residue. This loop region is of significance because of its proximity to the active site and because it contains two Tyr residues, Tyr605 and Tyr612, shown to be important in substrate binding and catalysis [15–17].

Previous studies have demonstrated that the Tyr612 hydroxyl is required for the efficient turnover of quenched fluorescent substrates [16,17]. For instance, the $k_{\text{cat}}/K_{\text{m}}$ value for the hydrolysis of mca-GlyPro-GlyPhe-dnp, a synthetic substrate, is decreased up to approximately 400-fold when Tyr612 is replaced with Phe [17]. The proposed role of Tyr612 of TOP is to stabilize the catalytic intermediate via hydrogen bond donation. This role is similar to that of other amino acid residues in peptidases, such as His231 in thermolysin [17,18]. However, modeling suggests that Tyr612 of TOP is several angstroms too far from the substrate in the crystallized conformation of the enzyme to effectively form hydrogen bonds [14,17].

It has been proposed that significant changes must occur, possibly on substrate binding, for Tyr605 and Tyr612 to be in appropriate positions to play their proposed roles in substrate catalysis [14–17]. Recently, the structure of the substrate/inhibitor bound form of DcP, a bacterial dipeptidyl carboxypeptidase from *Escherichia coli* bearing significant sequence similarity to TOP, has been elucidated [19]. Like TOP, DcP is bilobal, but, unlike TOP, the DcP structure is in a distinctly closed conformation. Using the structure of the carboxypeptidase DcP, we have produced a model for the closed form of TOP with bound substrate. The model allows for a more careful analysis of the residues in close proximity to the bound substrate in TOP, including Tyr612 and residues contained in the loop region 599–611 that join domain I and II. Supported by computational studies, activity assays with several structurally distinct substrates reveal a more significant catalytic role for Tyr605 than previously supposed

[15]. Furthermore, activity assays demonstrate that the quenched fluorescent analog of bradykinin requires neither Tyr residue for efficient turnover by TOP. This distinction among substrates has allowed for a careful analysis of the role of the conserved Gly residues in the 599–611 loop. The flexibility of the loop provides a means to bring Tyr612 and Tyr605 into close proximity to the bound substrate, and allows optimal substrate positioning by the enzyme. The evidence suggests that certain substrates require the formation of a closed form of the enzyme in order to be efficiently cleaved, whereas other substrates can be effectively utilized even by the open form of the enzyme. The possibility of alternative mechanisms of cleavage for different substrates has important implications for the physiological role of TOP and its wide distribution.

Results

Kinetic studies – Tyr mutants

The changes in the enzyme kinetic parameters of TOP towards four structurally distinct substrates on removal of the hydroxyl groups of Tyr605 and Tyr612 are shown in Table 1. The Y612F mutation resulted in a marked decrease in activity, as measured by changes in $k_{\text{cat}}/K_{\text{m}}$, with respect to wild-type activity towards 7-methoxycoumarin-4-acetyl-Pro-Leu-Gly-Pro-Lys-dinitrophenol (MCA), mcaNt and mca-Glu-His-Trp-Ser-Tyr-Gly-Leu-Arg-Pro-OH (mcaGnRH_{1–9}). The decrease was 1000- to 2000-fold with respect to mcaNt and MCA, and 200-fold with respect to mcaGnRH_{1–9}, and these changes were mostly a result of changes in k_{cat} . The Y605F mutation (Table 1) resulted in a lesser, but still considerable, 100-fold decrease in activity towards MCA and mcaNt, and a 12-fold decrease towards GnRH_{1–9}, again because of changes in k_{cat} . Interestingly, the Y605F mutant did not show significant changes in $k_{\text{cat}}/K_{\text{m}}$ with the 7-methoxycoumarin-4-acetyl-[Ala⁷, Lys(dinitrophenol)⁹]-bradykinin (mcaBk) substrate; the parameters were very similar to that of the wild-type. There were significant changes, however, in $k_{\text{cat}}/K_{\text{m}}$ with the double Y605/612F mutation, and less change with the single Y612F mutation, most notably as a result of changes in K_{m} .

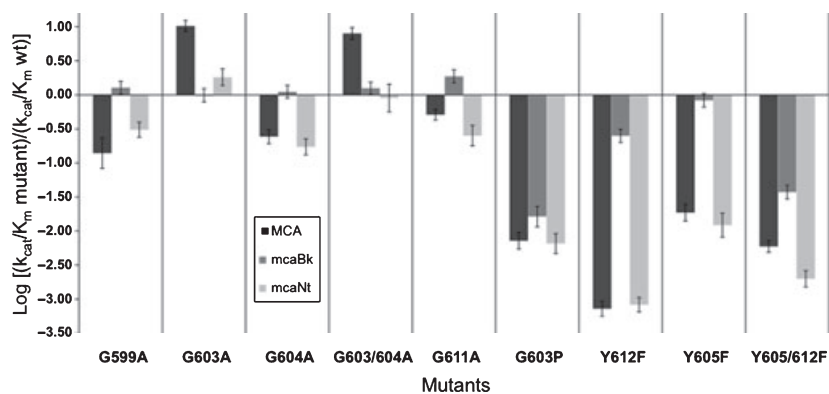
Gly mutants

Wild-type TOP has a clear preference for the mcaBk substrate over MCA and mcaNt based on $k_{\text{cat}}/K_{\text{m}}$ values (Table 1; Fig. 1). The majority of single substitutions of Ala for Gly in the loop region further

Table 1. Enzyme kinetics. Kinetic parameters of enzymes with four substrates.

Enzyme	k_{cat} (s^{-1})	K_{m} (μM)	$k_{\text{cat}}/K_{\text{m}}$ ($\mu\text{M}^{-1}\cdot\text{s}^{-1}$)
MCA			
Wild-type	0.44 ± 0.05	7.88 ± 1.03	0.05 ± 0.01
G599A	0.03 ± 0.01	4.08 ± 1.81	0.007 ± 0.003
G603A	2.32 ± 0.06	4.01 ± 0.21	0.58 ± 0.03
G604A	0.11 ± 0.01	8.25 ± 1.04	0.013 ± 0.002
G603A/G604A	2.44 ± 0.12	5.43 ± 0.39	0.45 ± 0.04
G611A	0.193 ± 0.002	6.7 ± 0.2	0.029 ± 0.001
G603P	0.0026 ± 0.0003	6.43 ± 1.22	0.00041 ± 0.00009
Y605F	0.0086 ± 0.001	8.2 ± 1.6	0.0011 ± 0.0002
Y612F	0.00037 ± 0.00004	9.0 ± 1.3	0.000041 ± 0.000007
Y605/612F	0.0023 ± 0.000002	8.1 ± 0.7	0.00028 ± 0.00002
mcaBk			
Wild-type	0.30 ± 0.05	0.057 ± 0.007	5.9 ± 1.1
G599A	0.86 ± 0.02	0.129 ± 0.009	6.7 ± 0.5
G603A	0.280 ± 0.004	0.054 ± 0.004	5.2 ± 0.5
G604A	0.53 ± 0.02	0.09 ± 0.05	5.8 ± 0.4
G603A/G604A	0.270 ± 0.001	0.041 ± 0.001	6.59 ± 0.14
G611A	1.34 ± 0.05	0.136 ± 0.010	9.8 ± 0.8
G603P	0.18 ± 0.05	2.1 ± 0.3	0.09 ± 0.02
Y605F	0.34 ± 0.01	0.08 ± 0.01	4.4 ± 0.4
Y612F	0.75 ± 0.02	0.57 ± 0.04	1.3 ± 0.11
Y605/612F	0.10 ± 0.003	0.51 ± 0.05	0.20 ± 0.02
mcaNt			
Wild-type	0.33 ± 0.03	1.2 ± 0.3	0.28 ± 0.07
G599A	0.18 ± 0.01	2.5 ± 0.2	0.07 ± 0.01
G603A	1.26 ± 0.05	2.9 ± 0.4	0.43 ± 0.06
G604A	0.11 ± 0.01	2.6 ± 0.3	0.04 ± 0.01
G603A/G604A	1.22 ± 0.27	5.7 ± 1.9	0.21 ± 0.08
G611A	0.30 ± 0.05	5.0 ± 1.0	0.06 ± 0.02
G603P	0.00449 ± 0.0005	2.9 ± 0.6	0.0016 ± 0.00037
Y605F	0.012 ± 0.002	4.2 ± 1.2	0.0029 ± 0.001
Y612F	0.00052 ± 0.00001	2.6 ± 0.1	0.0002 ± 0.00001
Y605/612F	0.0015 ± 0.0001	3.1 ± 0.38	0.00047 ± 0.00007
mcaGnRH₁₋₉			
Wild-type	11.2 ± 0.9	24 ± 4	0.47 ± 0.11
Y612F	0.061 ± 0.003	34 ± 3	0.0018 ± 0.0002
Y605F	1.4 ± 0.2	37 ± 10	0.038 ± 0.02
Y605/612F	0.025 ± 0.001	14 ± 1	0.0017 ± 0.002

Fig. 1. Comparison of $k_{\text{cat}}/K_{\text{m}}$ of mutants with $k_{\text{cat}}/K_{\text{m}}$ of wild-type for three substrates. $k_{\text{cat}}/K_{\text{m}}$ for each mutant with MCA, mcaBk and mcaNt, where wild type = 0 on the logarithmic scale.



increased this selectivity by considerably decreasing the activity towards the MCA and mcaNt substrates, while generally having no effect or a slight improvement in activity towards mcaBk. This effect was observed for the MCA and mcaNt substrates with the G599A, G604A and G611A mutant forms. For instance, each enzyme showed decreased overall activity towards mcaNt as a result of decreased k_{cat} values when compared with the wild-type, except for G611A which showed a k_{cat} value similar to that of the wild-type. Indeed, both G599A and G604A showed changes in K_{m} that were consistent with the changes in k_{cat} : about threefold for k_{cat} and about twofold for K_{m} . That is, changes in activity towards the mcaNt substrate were a result of changes seen in both constants, although somewhat more for k_{cat} , whereas those towards MCA were purely a result of changes in k_{cat} .

However, the substitution of Ala for Gly at position 603 in either single or double mutations notably altered the preference of the enzyme (Fig. 1; Table 1). G603A had the effect of creating a greater preference for the five-residue MCA substrate and, to a lesser extent, for the 10-residue mcaNt substrate compared with the wild-type and all other single mutants. The double mutant that combined the G603A substitution with a second Ala substitution (G604A) retained increased activity towards MCA. Activity for the double mutant towards the Nt derivative did not increase compared with the wild type, although its activity was notably higher than that of the single G604A mutant.

Although the substitution of Ala for Gly at position 603 led to enhanced activity towards MCA and mcaNt, substitution of Pro for Gly caused a significant decrease in $k_{\text{cat}}/K_{\text{m}}$ with MCA and mcaNt. The decrease in activity was approximately 1000-fold with MCA and approximately 200-fold with mcaNt, both primarily caused by a decrease in k_{cat} .

Data for the loop mutants further demonstrated that the mcaBk substrate was distinct (Table 1). This substrate showed only little to no change in activity with the loop Gly mutants. Only G611A, the mutation closest to Tyr612, resulted in any substantial effect on the activity towards mcaBk. The G603A and G604A mutations, both of which lie close to Y605, caused no significant change in activity towards mcaBk. It is notable that Y612F and Y605F caused a modest and no change, respectively, towards this same substrate. Substitution of Pro for Gly at position 603 led to significant decreases in activity for the mcaBk substrate. In contrast with the other mutants, the change for the Pro substitution was entirely a result of changes in K_{m} , not k_{cat} .

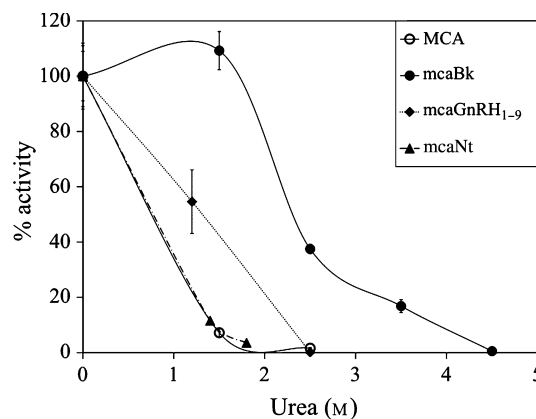


Fig. 2. Percentage activity of wild-type TOP with the substrates MCA, mcaBk, mcaGnRH₁₋₉ and mcaNt in the presence of increasing urea (M).

Denaturing activity trends

Previously, we have reported changes in activity of two of the substrates (MCA and mcaBk) at low urea concentrations [20]. Here, we expand on those data with two additional structurally distinct and physiologically relevant, neuropeptide-based substrates (Fig. 2). Similar to the Tyr mutations, urea had distinct effects on mcaBk, which were not apparent for the other substrates tested. At low urea concentrations, TOP lost activity towards MCA, mcaNt and mcaGnRH₁₋₉. However, the enzyme was fully active towards mcaBk, even between 1 and 2 M urea. Interestingly, the trends in activity in urea paralleled the trends observed with the Y612F mutant. For mcaBk, which suffered an increase in K_{m} with the Y612F mutant, low urea caused an increase in K_{m} and k_{cat} . Between 1 and 2 M urea, the Y612F enzyme also retained marked activity towards mcaGnRH₁₋₉. Both MCA and mcaNt, the most sensitive to the Y612F mutation, showed the largest decrease in activity between 1 and 2 M urea. Above 3 M urea, the enzyme lost activity to all substrates as a result of enzyme denaturation and zinc(II) loss from the active site [20].

HPLC analysis

To determine whether the change in activity towards MCA and mcaNt substrates was caused by a change in substrate recognition by the modified enzymes, resulting in an altered cleavage site, wild-type TOP and MCA were incubated for 30 min and the products were evaluated by HPLC. Two products with an absorbance at 330 nm were detected, suggesting a single cleavage site in the MCA substrate. Extended incubation and examination of the products of

mcaNt after 90 min revealed four products, leading to suggestions of additional cleavage sites for the mcaNt substrate. Identical results were obtained concerning the position of cleavage sites for the Gly mutants (data not shown).

Modeling and molecular simulations of wild-type and mutant TOP

By analogy with the DcP enzyme [19], the transition between the open (substrate-free) and closed (substrate-bound) forms of TOP probably occurs through a reorientation of domains I and II. Thus, a model of the closed form of TOP was created by separately fitting domains I and II of the open TOP crystal structure onto the structure of DcP in its closed form [19]. The TOP domains superimposed very well on the DcP structure, with rms deviations of 1.50 and 1.21 Å for domains I and II, respectively. After fitting and minimization, the closed model of TOP was quite similar to that of DcP, indicating that the two domains of TOP form relatively rigid structures that change their relative orientation by pivoting on residues 156, 351, 544 and 616 connecting the two lobes. Modeling TOP onto DcP moved several domain II Tyr residues of TOP, known to be involved in catalysis or substrate binding [17,19], into positions analogous to those of closed DcP, and thus to the appropriate distances from the active site to perform such roles (Fig. 3). Tyr605 and Tyr609 fall within the loop structure, whereas Tyr612 is just at the end of the loop. The original substrate-free structure of TOP showed that Tyr612, an important catalytic residue based on mutagenesis

studies [17], is more than 8 Å from the active site. The closed form orients the phenol oxygen of this residue within hydrogen bonding distance from the carboxyl group of the scissile peptide bond in a modeled substrate. Furthermore, Tyr605 and Tyr609, both implicated in substrate binding, are shown in Fig. 3 to be within hydrogen bonding distance from the substrate.

As energy minimization only allows for limited conformational sampling, we also subjected our TOP model to a molecular dynamics simulation in explicit solvent in order to sample additional conformations of the substrate and the enzyme. Although all residues were allowed to move freely in these simulations, the overall enzyme structure and the loop region maintained relatively low C α rms deviations from our initial model throughout this trajectory (< 3.0 and < 1.5 Å, respectively). The substrate also maintained its relative position in the active site during the simulation. These data do not preclude the existence of other possible conformations further away from the starting model that were not sampled during the molecular dynamics simulation. However, significant structural homology between TOP and DcP around the active site residues of domain I and the loop and Tyr residues in domain II supports our initial conformation for the model. Furthermore, the experimental effects observed for Tyr605 and Tyr612 mutants on enzyme activity validate the close proximity of these residues to the substrate in the model.

The molecular dynamics simulations on wild-type TOP and all four Gly mutants (G599A, G603A, G604A and G611A) also provide an insight into how Ala mutations affect the structure and dynamics of the loop region. All of these simulations included an MCA-like substrate in the active site (Fig. 3). As expected, based on the flexibility of Gly, all four Ala mutations led to decreased structural flexibility in the loop region. For example, the loop region in the wild-type enzyme showed an increased C α rms fluctuation over the final nanoseconds of the trajectories in the Gly-rich region of the loop between residues 599 and 604 (data not shown). In addition, the wild-type loop showed an ability to more readily access a wider variety of conformations. This was particularly true for the section of the loop between residues 605 and 612, which contains the Tyr residues demonstrated to be important for catalysis in this study. This region had a greater average C α rms deviation (2.7 Å) from the initial model over the last nanoseconds of the simulation than observed in mutant simulations (1.2–1.95 Å). This increased conformational sampling also led the wild-type simulation to show reduced hydrogen bonding between loop residues and the substrate (Table 2) at

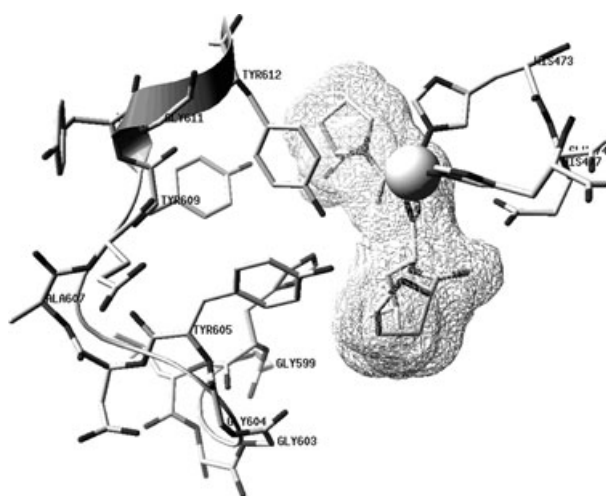


Fig. 3. Molecular model of TOP used as the initial structure for molecular dynamics simulations of wild-type, G603A and G604A TOP with the MCA substrate shown in space filling.

Table 2. Percentage of hydrogen bonding distances of the mutants. The percentage of hydrogen bonding that occurred in the last nanosecond was calculated by looking at every 10 ps frame. The average minimum distance between the side-chain hydroxyl oxygen of Tyr residues and MCA is given in brackets. The data were calculated from the molecular dynamics simulations described in Fig. 3. Distances and percentage hydrogen bonding for all mutants were calculated based on the last nanosecond of the trajectories. All simulations were run for 10 ns, except for G604A which was run for 15 ns.

	Hydrogen bonding (%) in last nanosecond [average distance (nm) between Tyr and MCA-like substrate]		
	Y605–MCA	Y609–MCA	Y612–MCA
Wild-type	11 [0.30]	0 [0.70]	0 [0.34]
G599A	5 [0.34]	0 [0.44]	66 [0.23]
G603A	3 [0.33]	73 [0.31]	69 [0.21]
G604A	83 [0.26]	73 [0.21]	0 [0.32]
G611A	0 [0.41]	0 [0.37]	0 [0.31]

the end of the simulation, despite having a close proximity between Tyr hydroxyl groups (e.g. 2–3 Å) and the substrate in the initial model.

In addition to reducing the flexibility of the loop, different Ala substitutions led to different hydrogen bonding patterns between Tyr residues in the loop and the substrate (Table 2). Thus, in addition to generally decreasing flexibility, the Ala mutants may restrict the loop to different conformations relative to the substrate. It would be tenuous to interpret these hydrogen bonding results too strongly in terms of catalysis, as the simulations have a relatively short time scale (10–15 ns) and include a substrate-like molecule that would not necessarily mimic enzyme interactions in the transition state. For example, Tyr residues in the loop of wild-type TOP clearly have the ability to interact with the substrate during catalysis, although the loop sampled conformations further from the substrate in the wild-type simulation. Nonetheless, these results imply that conformational differences caused by different Ala substitutions could lead to differences in experimentally observed kinetic data, such as the increased activity of G603A towards MCA compared with the adjacent G604A mutation. Moreover, Tyr609 formed hydrogen bonds with the substrate in several trajectories. It would be interesting for future studies to consider the possible role of this residue in catalysis in more detail.

Discussion

A major finding of this study is that the bradykinin analogue mcaBk can still be cleaved efficiently after

removal of the Tyr hydroxyls of Y605 and Y612 from the wild-type form of the enzyme, thus making this substrate distinct among the four substrates tested. This discovery helped reveal the primary role of Gly residues in the 599–611 loop in positioning the Tyr605 and Tyr612 residues needed for substrate hydrolysis. In addition, our data indicate that Tyr605 is responsible for transition state stabilization by hydrogen bonding interactions with the substrate.

Role of Tyr605 and Tyr612 in catalysis

Activity assays and molecular modeling support a direct role for both Tyr605 and Tyr612 in peptide hydrolysis by TOP. Previous data demonstrating the crucial role of Tyr612 in the cleavage of the quenched fluorescent substrate MCA [16,17] was corroborated and expanded upon in this study with two additional physiologically related substrates, mcaNt and mcaGnRH_{1–9}. Removal of the Tyr hydroxyl in the Y612F mutant resulted in a 500- to 2000-fold decrease in k_{cat} for these three substrates (see Table 1). Molecular modeling of the closed form of TOP showed that the hydroxyl of Tyr612 is within hydrogen bonding distance of the carbonyl carbon of the cleaved peptide bond. Tyr605 also seems to play a significant, although lesser, role than Tyr612. The Y605F mutant suffered a 10–200-fold decrease in k_{cat} for hydrolysis of MCA, mcaNt and mcaGnRH_{1–9}. In a previous study, Machado *et al.* [15] determined that Tyr605 drives substrate specificity via an interaction at the P1 residue of the bradykinin-based substrate *O*-aminobenzoyl-Gly-Phe-Ser (X is one of several amino acid substitutions)-Phe-Arg-Gln-*N*-(2,4-dinitrophenyl)-ethylenediamine. However, no clear effect on k_{cat} was observed, and thus no direct catalytic role was assigned to Tyr605. From the present study, it appears that Tyr605 does play a significant role, as shown by the large decrease in k_{cat} with MCA and mcaNt. It is possible that Tyr605 may position certain substrates; without Tyr605, the peptide is no longer in the appropriate position with respect to Tyr612. Alternatively, Tyr605 may be more directly involved in catalysis, as shown by the changes seen in $k_{\text{cat}}/K_{\text{m}}$ with the single Tyr mutant. Molecular modeling and molecular dynamics indeed suggest that the Tyr605 hydroxyl is in close proximity to the carbonyl of the scissile peptide bond. Therefore, Tyr605 is probably also responsible for transition state stabilization, suggested previously for the Tyr612 residue [16]. This coordinated effort is similar to that of His231 and Tyr157 in thermolysin [21,22]. His231 (analogous to Tyr612 in TOP) and Tyr157 (analogous to Tyr605 in TOP) work together in the

transition state stabilization of this enzyme, both forming hydrogen bonds to the transition state intermediate [21,22]. In thermolysin, His231 plays the dominant role to Tyr157, the removal of which results in a decrease in activity of approximately 200-fold. This is comparable with the relative roles played by Tyr612 and Tyr605 mutants of TOP, where Y612F suffers a 500- to 2000-fold decrease in activity relative to the wild-type, and Y605F shows a 10- to 200-fold decrease. This rotation and approach of hydrogen bonds by Tyr residues have been seen in other peptidases, such as *Thermoplasma acidophilum* aminopeptidase factor F3, *Saccharomyces cerevisiae* and human dipeptidyl peptidase III (DPP III), indicating similar transition state stabilizations during the catalytic event [21,23–26].

Possibility that mcaBk could be cleaved by an open form of the enzyme

The most surprising finding from this study was that TOP does not require either Tyr605 or, more significantly, Tyr612 for significant activity towards the mcaBk substrate (see Table 1). Y612F caused only a slight increase in K_m for this substrate. Virtually no change in the kinetic parameters for TOP with mcaBk was detected on removal of the Tyr605 hydroxyl, especially when compared with the 10- to 100-fold change with the other substrates tested (see Table 1). Although the enzyme showed a significant decrease in activity towards the mcaBk substrate when both Tyr605 and Tyr612 hydroxyls were removed, it still retained considerable activity. k_{cat}/K_m for mcaBk with the double Tyr mutant was $0.20 \mu\text{M}^{-1}\cdot\text{s}^{-1}$ (Table 1), comparable with the rate constants for mcaNt and mcaGnRH_{1–9} with the wild-type (0.28 and $0.37 \mu\text{M}^{-1}\cdot\text{s}^{-1}$). Clearly, hydrolysis of mcaBk does not absolutely require these Tyr residues. This observation suggests that the enzyme may not need to be in the closed conformation to process mcaBk, or that the mechanism of cleavage of mcaBk is altered with respect to that of the other substrates. The first suggestion is supported by the significant activity retained towards mcaBk in the presence of low concentrations (1–2 M) of urea (Fig. 2). Previous fluorescence data imply that this concentration of urea favors either denaturation of domain II or at least an open conformation of the enzyme [20]. This finding is significant, as the open–closed hinge mechanism is likely to be the key factor in limiting substrate length.

The movement of flexible hinge regions to modulate the open–closed scenario has been demonstrated in a variety of metallopeptidases and their intermediate forms [27–29]. The majority of TOP substrates tested can only be hydrolyzed when the loop region is in the

closed conformation, which brings Tyr605 and Tyr612 into the appropriate position. No other Tyr residues or possible hydrogen bond donors are apparent in the structure of the TOP enzyme. Based on the structure of the carboxypeptidase DcP [19], this complete closure of the crevice is needed for efficient catalysis, because it causes the internal crevice to be inaccessible from the outside. However, if TOP can remain in the open position for certain substrates, as suggested in this study with mcaBk, it may be possible that, under certain conditions, this enzyme can cleave larger (> 17 amino acid) substrates, such as peptides that function in cell signaling [30].

The open–closed conformational change also opens up the possibility for an additional mechanism to regulate TOP's activity. Certain Cys residues of TOP are known to be involved in thiol activation/*S*-glutathionylation, promoting an oligomerized enzyme with reduced enzyme activity [31–33]. It is possible that oxidation and the open–closed transition are connected, and that thiol oxidation forces the enzyme into a closed state.

Role of Gly residues of the 599–611 loop in positioning Tyr605 and Tyr612

Previous work has suggested that the flexible loop region of TOP is responsible for this enzyme's positioning of substrates for catalysis [15]. The present results clarify the primary role of the Gly residues of TOP to be the positioning of Tyr605 and Tyr612. This is supported by the fact that hydrolysis of mcaBk, which changed very little when the Tyr residues were mutated, was also relatively unaffected by the mutation of Gly residues in the 599–611 loop (Table 1).

This is in contrast with the other substrates used in this study, all of which showed a significant decrease in k_{cat} on removal of either Tyr605 or Tyr612. Further, activities against MCA and mcaNt were affected to a significant degree by either the single or double Gly mutations in the loop. The G604A and G603A mutations, as well as the Y605F single mutation, had no effect on activity towards mcaBk, whereas the change in activity of Gly611 towards mcaBk was mirrored by the small change in activity of the Y612F mutant. These results may point to a specific role for the Gly residues in the positioning of Tyr605 and Tyr612, and also suggest the coordinated role played by these loop Gly residues in the selection of substrates. The molecular dynamics simulations also support a role of these Gly residues in positioning of the catalytic Tyr residues.

Previous work [16], in which Ala607 of the 599–611 substrate-binding loop in TOP was changed to Gly

(the corresponding residue in neurolysin), demonstrated that this residue may be important in governing the differences in substrate selection by these two enzymes. However, it seems unlikely that the residue in this position of the loop is responsible for allowing TOP to adopt an active conformation, as this position is not conserved between the two enzymes. Both enzymes bind and hydrolyze a diverse array of peptides, often at the same cleavage site. Rather, the evidence in this paper supports a role for the conserved Gly residues (599, 603, 604, 611) in the loop, particularly Gly603, in maintaining the plasticity of the active site and the full range of function of TOP. Most recently [30], potential new substrates adhering to the size specificity ascribed to TOP have been described. These are consistent with the findings of the role of the Gly substrate-binding loop.

To conclude, our study presents evidence that particular amino acids in the catalytic loop region of TOP are crucial for positioning important Tyr residues involved in the catalysis of physiologically relevant peptides. In addition, the mechanism for catalysis employed by TOP determines this enzyme's success with a wide variety of substrates.

Materials and methods

Reagents

The quenched fluorescent substrates MCA and modified bradykinin (mcaBk) were purchased from Bachem (King of Prussia, PA, USA). Modified neurotensin (mca-Leu-Tyr-Glu-Asn-Lys-Pro-Arg-Arg-Pro-Lys(Dnp)-OH) and mca-GnRH₁₋₉ were synthesized by AnaSpec (San Jose, CA, USA). tris(2-Carboxyethyl)phosphine hydrochloride (TCEP) was obtained from Pierce Chemical Co. (Rockford, IL, USA). All other chemicals were purchased from Sigma Chemical Co. (St Louis, MO, USA).

Mutagenesis and protein expression

Site-directed mutagenesis of rat EP24.15 was performed on the expression vector pGEX-24.15 as a template [34]. Oligonucleotide primers were synthesized with mismatches, coding for the appropriate amino acid change following prokaryotic codon usage rules to obviate the use of rare codons. Mutations were performed using separate forward (Fw) and reverse (Rv) primers: FwRepG611A (TACGACGCTCAGTACTATGCTTACTTGTGGAGTGAGGTG); RvRepG611A (CACCTCACTCCACAAGTAAGCATAGTACTGAGCGTCGTA); FwRepG603A (CTTTTGGCCACCTCGCTGCTGGCTACGACGCTCAGTAC); RvRepG603A (GTACTGAGCGTCGTAGCCAGCAGCGAGGTG

GCCAAAAG); FwRepG604A (GGCCACCTCGCTGGTGCTACGACGCTCAGTAC); RvRepG604A (GTAAGTGA GCGTCGTAGGCACCAGCGAGGTGGCC); FwRepG599A (CAACATGCCAGCCACTTTTGGCCACCTCGCTGGTGGCTACG); RvRepG599A (CGTAGCCACCAGC GAGGTGGGCAAAAGTGGCTGGCATGTTG); FwRepY605F (CCACCTCGCTGGTGGC TTCGACGCTCAG TACTATG); RvRepY605F (CATAGTACTGAGCGTCG AAGCCACCAGCGAGGTGG); FwRepY609F (GGCTA CGACGCTCAGTTCTATGGCTACTTGTGG); RvRepY609F (CCACAAGTAGCCATAGAAGTACTGAGCGTCGT AGCC); FwRepY612F (GCTCAGTACTATGGCTTCTT GTGGAGTGAGGTG); RvRepY612F (CACCTCACTCC ACAAGAAGCCATAGTACTGAGC); FwRepG603P (CT TTTGGCCACCTCGCTCCCGGCTACGACGCTCAGTA); RvRepG603P (TACTGAGCGTCGTAGCCGGGAGCGA GGTGGCCAAAAG). All constructs were sequenced to ensure that the correct mutation was created.

The assessment of purification to homogeneity, yield and appropriate folding of expressed proteins was by native PAGE on an 8% gel under reducing conditions, as described previously [35]. Yields of expressed protein were similar for all of the mutations.

To determine whether gross structural alterations occurred during mutagenesis and subsequent protein expression, mutants were compared with the wild-type by CD spectroscopy. CD spectra were collected in the wavelength range 300–185 nm at 1 nm intervals with a Jasco 715 spectropolarimeter (Jasco, Easton, MD, USA). The instrument wavelength was checked with benzene vapor. Optical rotation was calibrated by measuring the ellipticity of d-10 camphorsulfonic acid at 192.5 and 290 nm. Measurements of optical ellipticity were made at 25 °C using a quartz cell (path length, 0.1 cm). At least eight reproducible scans were collected for each sample. Buffer alone was used for a control blank in these experiments, and the averaged buffer spectrum was subtracted from each averaged protein spectrum. The contribution of the polypeptide component alone was similar for all of the mutations compared with the wild-type protein.

Kinetic assays

Kinetic assays were performed as described previously [20]. Cleavage of the fluorogenic MCA [36], mcaBk and mcaNt substrates was monitored by the increase in emission at 400 nm over time using $\lambda_{\text{excitation}} = 325 \text{ nm}$. The mcaGnRH₁₋₉ substrate was monitored by HPLC (Agilent 1100) using the increase in peak area for the emission of mca at 400 nm with $\lambda_{\text{excitation}} = 325 \text{ nm}$. Assays were performed at least in duplicate at 23 °C in 25 mM Tris/HCl at pH 7.8, containing 1 mM TCEP, 1 μM ZnCl₂, and 10% glycerol, adjusted to a conductivity of 12 $\text{mS}\cdot\text{cm}^{-2}$ with NaCl.

The kinetic parameters were determined using a hyperbolic fit to the plot of substrate concentration versus rate of product formation. All curve-fitting procedures were performed using the program T-CURVE 2D (SPSS Inc., Chicago, IL, USA).

HPLC analysis

Products of the enzymatic reaction of wild-type and mutant TOP with substrates MCA and mcaNt were analyzed using HPLC (Hewlett Packard 1090, Palo Alto, CA, USA). The reaction mixture, 50 μ L total volume in Tris buffer, contained either MCA (350 μ M) and 0.4 μ M of enzyme, or mcaNt (100 μ M) and 0.9 μ M of enzyme. A sample was taken at 0 min (before initiation of the reaction) and after reaction for 90 min at room temperature. Each reaction was terminated with the addition of equal volumes of 0.1% trifluoroacetic acid in methanol.

A 20 μ L aliquot of the reaction mixture was subjected to reverse-phase HPLC using a C18 3 μ m column (150 mm \times 4.6 mm; Alltech, Bannockburn, IL, USA) at a flow rate of 1 mL \cdot min $^{-1}$ with a linear gradient of 10–66% acetonitrile in 0.1% trifluoroacetic acid. The elution of substrates and products was monitored by absorbance at 330 nm [20].

Modeling and molecular dynamics simulations

An initial model of TOP with bound MCA (Pro-Leu-Gly-Pro) substrate was based on the TOP crystal structure (PDB ID # 1s4b) [14], with the loop conformation modified analogously to a structure of DcP (PDB ID # 1y79) that has product bound in the active site [19]. Specifically, a model of the closed form of TOP was generated by clipping TOP at the division between domains I and II (residues Leu156, Val351, Gln544 and Glu616), and separately fitting domains I and II to the structure of DcP. The identification of the appropriate clipping points was aided by using the Alternate Domain Fit tool from the suite of tools within the SWISS-PDBVIEWER (<http://www.expasy.org/spdbv/>) software version 3.7 and 3.9b2 [37]. The fitting procedure was accomplished by two methods with similar overall results. Fitting the entirety of the domains using Bestfit with structure alignment resulted in a total rms backbone deviation of 1.52 Å. After fitting the domains, the TOP backbone was re-ligated. Alternatively, the zinc and active site residues could be overlain to fit domain I and the conserved His600, Tyr605 and Tyr612 of TOP used to fit domain II. The second procedure resulted in a similar rms backbone deviation of 1.51 Å with a slightly better fit of the active site residues. G603A and G604A mutations were made to this minimized model.

Molecular dynamics simulations of wild-type, G599A, G603A, G604A and G611A TOP were performed and analyzed using the GROMACS 3.3.1 suite [38]. TOP models were

solvated in a cubic box of 41 111 simple point charge water molecules with Na $^{+}$ and Cl $^{-}$ ions to neutralize the system and provide a salt concentration of 100 mM. These solvated models were subjected to 50 steps of steepest descent minimization and were heated to 298 K over 20 ps. Initial position restraints on all C α atoms were released in gradual steps over the first 275 ps of the 10 ns trajectories. Temperature (298 K) and pressure (1 bar) were controlled using Berendsen coupling protocols with time constants of 0.1 ps and 1.0 ps, respectively [39]. Electrostatic and Lennard–Jones' interactions were cut off at 10 Å with long-range electrostatics computed using Particle Mesh Ewald (PME) [40]. Bonds were constrained with the LINCS algorithm [41]. Distance restraints analogous to those used for other metalloenzyme simulations [42] were employed to maintain interactions between Zn $^{2+}$ and His473, His477 and Glu502. Properties were averaged over the last nanoseconds of trajectories, and hydrogen bonds were defined geometrically with a donor–acceptor distance cut-off of 3.5 Å and an angle cut-off of 30°.

Acknowledgements

We thank Meera Srikanthan, Lindsay Kua, Connie Wu, Susan Kim and Sabina Khan for technical assistance. We also thank Didem Vardar-Ulu for technical advice. This study was supported by a Howard Hughes Medical Institute Undergraduate Education Program Grant, a National Science Foundation (NSF) Research Experiences for Undergraduate Award to Wellesley College (CHE-0353813), the National Institute for Neurological Disorders and Stroke (NS39892) of the National Institutes of Health (MJG), and the Camille and Henry Dreyfus Supplemental Research Grant under the Scholar/Fellow Program (JAS).

References

- 1 Rawlings ND & Barrett AJ (1993) Evolutionary families of peptidases. *Biochem J* **290**, 205–218.
- 2 Pierotti A, Dong KW, Glucksman MJ, Orłowski M & Roberts JL (1990) Molecular-cloning and primary structure of rat testes metalloendopeptidase Ec 3.4.24.15. *Biochemistry* **29**, 10323–10329.
- 3 Dauch P, Vincent JP & Checler F (1995) Molecular-cloning and expression of rat-brain endopeptidase-3.4.24.16. *J Biol Chem* **270**, 27266–27271.
- 4 Brown CK, Madauss K, Lian W, Beck MR, Tolbert WD & Rodgers DW (2001) Structure of neurolysin reveals a deep channel that limits substrate access. *Proc Natl Acad Sci USA* **98**, 3127–3132.
- 5 Ray K, Hines CS & Rodgers DW (2002) Mapping sequence differences between thimet oligopeptidase and

- neurolysin implicates key residues in substrate recognition. *Protein Sci* **11**, 2237–2246.
- 6 Dando PM, Brown MA & Barrett AJ (1993) Human thimet oligopeptidase. *Biochem J* **294**, 451–457.
 - 7 Rioli V, Gozzo FC, Heimann AS, Linardi A, Krieger JE, Shida CS, Almeida PC, Hyslop S, Eberlin MN & Ferro ES (2003) Novel natural peptide substrates for endopeptidase 24.15, neurolysin, and angiotensin-converting enzyme. *J Biol Chem* **278**, 8547–8555.
 - 8 Smith AI, Lew RA, Shrimpton CN, Evans RG & Abbenante G (2000) A novel stable inhibitor of endopeptidases EC 3.4.24.15 and 3.4.24.16 potentiates bradykinin-induced hypotension. *Hypertension* **35**, 626–630.
 - 9 Smith AI, Shrimpton CN, Norman UM, Clarke IJ, Wolfson AJ & Lew RA (2000) Neuropeptidases regulating gonadal function. *Biochem Soc Trans* **28**, 430–434.
 - 10 Akil H, Watson SJ, Young E, Lewis ME, Khachaturian H & Walker JM (1984) Endogenous opioids – biology and function. *Annu Rev Neurosci* **7**, 223–255.
 - 11 Portaro FC, Gomes MD, Cabrera A, Fernandes BL, Silva CL, Ferro ES, Juliano L & de Camargo AC (1999) Thimet oligopeptidase and the stability of MHC class I epitopes in macrophage cytosol. *Biochem Biophys Res Commun* **255**, 596–601.
 - 12 Silva CL, Portaro FC, Bonato VL, de Camargo AC & Ferro ES (1999) Thimet oligopeptidase (EC 3.4.24.15), a novel protein on the route of MHC class I antigen presentation. *Biochem Biophys Res Commun* **255**, 591–595.
 - 13 Kim SI, Pabon A, Swanson TA & Glucksman MJ (2003) Regulation of cell-surface major histocompatibility complex class I expression by the endopeptidase EC3.4.24.15 (thimet oligopeptidase). *Biochem J* **375**, 111–120.
 - 14 Ray K, Hines CS, Coll-Rodriguez J & Rodgers DW (2004) Crystal structure of human thimet oligopeptidase provides insight into substrate recognition, regulation, and localization. *J Biol Chem* **279**, 20480–20489.
 - 15 Machado MF, Rioli V, Dalio FM, Castro LM, Juliano MA, Tersariol IL, Ferro ES, Juliano L & Oliveira V (2007) The role of Tyr605 and Ala607 of thimet oligopeptidase and Tyr606 and Gly608 of neurolysin in substrate hydrolysis and inhibitor binding. *Biochem J* **404**, 279–288.
 - 16 Oliveira V, Araujo MC, Rioli V, de Camargo AC, Tersariol IL, Juliano MA, Juliano L & Ferro ES (2003) A structure-based site-directed mutagenesis study on the neurolysin (EC 3.4.24.16) and thimet oligopeptidase (EC 3.4.24.15) catalysis. *FEBS Lett* **541**, 89–92.
 - 17 Sigman JA, Edwards SR, Pabon A, Glucksman MJ & Wolfson AJ (2003) pH dependence studies provide insight into the structure and mechanism of thimet oligopeptidase (EC 3.4.24.15). *FEBS Lett* **545**, 224–228.
 - 18 Holland DR, Hausrath AC, Juers D & Matthews BW (1995) Structural-analysis of zinc substitutions in the active-site of thermolysin. *Protein Sci* **4**, 1955–1965.
 - 19 Comellas-Bigler M, Lang R, Bode W & Maskos K (2005) Crystal structure of the *E. coli* dipeptidyl carboxypeptidase Dcp: further indication of a ligand-dependent hinge movement mechanism. *J Mol Biol* **349**, 99–112.
 - 20 Sigman JA, Patwa TH, Tablante AV, Joseph CD, Glucksman MJ & Wolfson AJ (2005) Flexibility in substrate recognition by thimet oligopeptidase as revealed by denaturation studies. *Biochem J* **388**, 255–261.
 - 21 Marie-Claire C, Ruffet E, Tiraboschi G & Fournie-Zaluski MC (1998) Differences in transition state stabilization between thermolysin (EC 3.4.24.27) and nepri-lysin (EC 3.4.24.11). *FEBS Lett* **438**, 215–219.
 - 22 Holden HM & Matthews BW (1988) The binding of L-valyl-L-tryptophan to crystalline thermolysin illustrates the mode of interaction of a product of peptide hydrolysis. *J Biol Chem* **263**, 3256–3260.
 - 23 Yiallourous I, Berkhoff EG & Stocker W (2000) The roles of Glu93 and Tyr149 in astacin-like zinc peptidases. *FEBS Lett* **484**, 224–228.
 - 24 Kyrieleis OJ, Goettig P, Kiefersauer R, Huber R & Brandstetter H (2005) Crystal structures of the tricorn interacting factor F3 from *Thermoplasma acidophilum*, a zinc aminopeptidase in three different conformations. *J Mol Biol* **349**, 787–800.
 - 25 Thompson MW, Archer ED, Romer CE & Seipelt RL (2006) A conserved tyrosine residue of *Saccharomyces cerevisiae* leukotriene A(4) hydrolase stabilizes the transition state of the peptidase activity. *Peptides* **27**, 1701–1709.
 - 26 Salopek-Sondi B, Vukelic B, Spoljaric J, Simaga S, Vujaklija D, Makarevic J, Jajcanin N & Abramic M (2008) Functional tyrosine residue in the active center of human dipeptidyl peptidase III. *Biol Chem* **389**, 163–167.
 - 27 Okoniewska M, Tanaka T & Yada RY (2000) The pepsin residue glycine-76 contributes to active-site loop flexibility and participates in catalysis. *Biochem J* **349**, 169–177.
 - 28 Kempner ES (1993) Movable lobes and flexible loops in proteins – structural deformations that control biochemical-activity. *FEBS Lett* **326**, 4–10.
 - 29 Tanaka T, Yamaguchi H, Kato H, Nishioka T, Katsube Y & Oda J (1993) Flexibility impaired by mutations revealed the multifunctional roles of the loop in glutathione synthetase. *Biochemistry* **32**, 12398–12404.
 - 30 Cunha FM, Berti DA, Ferreira ZS, Klitzke CF, Markus RP & Ferro ES (2008) Intracellular peptides as natural regulators of cell signaling. *J Biol Chem* **283**, 24448–24459.
 - 31 Shrimpton CN, Glucksman MJ, Lew RA, Tullai JW, Margulies EH, Roberts JL & Smith AI (1997) Thiol activation of endopeptidase EC 3.4.24.15. A novel

- mechanism for the regulation of catalytic activity. *J Biol Chem* **272**, 17395–17399.
- 32 Demasi M, Piassa Filho GM, Castro LM, Ferreira JC, Rioli V & Ferro ES (2008) Oligomerization of the cysteinyl-rich oligopeptidase EP24.15 is triggered by S-glutathionylation. *Free Radic Biol Med* **44**, 1180–1190.
- 33 Sigman JA, Sharky ML, Walsh ST, Pabon A, Glucksman MJ & Wolfson AJ (2003) Involvement of surface cysteines in activity and multimer formation of thimet oligopeptidase. *Protein Eng* **16**, 623–628.
- 34 Glucksman M & Roberts JL (1995) Strategies for characterizing, cloning and expressing soluble endopeptidases. *Methods Neurosci* **23**, 296–316.
- 35 Cummins PM, Pabon A, Margulies EH & Glucksman MJ (1999) Zinc coordination and substrate catalysis within the neuropeptide processing enzyme endopeptidase EC 3.4.24.15. Identification of active site histidine and glutamate residues. *J Biol Chem* **274**, 16003–16009.
- 36 Wolfson AJ, Shrimpton CN, Lew RA & Smith AI (1996) Differential activation of endopeptidase EC 3.4.24.15 toward natural and synthetic substrates by metal ions. *Biochem Biophys Res Commun* **229**, 341–348.
- 37 Guex N & Peitsch MC (1997) SWISS-MODEL and the Swiss-Pdb Viewer: an environment for comparative protein modeling. *Electrophoresis* **18**, 2714–2723.
- 38 Lindahl E, Hess B & van der Spoel D (2001) GRO-MACS 3.0: a package for molecular simulation and trajectory analysis. *J Mol Model* **7**, 306–317.
- 39 Berendsen HJC, Postma JPM, Vangunsteren WF, Dinola A & Haak JR (1984) Molecular-dynamics with coupling to an external bath. *J Chem Phys* **81**, 3684–3690.
- 40 Darden T, York D & Pedersen L (1993) Particle Mesh Ewald – an N.Log(N) method for Ewald sums in large systems. *J Chem Phys* **98**, 10089–10092.
- 41 Hess B, Bekker H, Berendsen HJC & Fraaije J (1997) LINCS: A linear constraint solver for molecular simulations. *J Comput Chem* **18**, 1463–1472.
- 42 Manzetti S, McCulloch DR, Herington AC & van der Spoel D (2003) Modeling of enzyme–substrate complexes for the metalloproteases MMP-3, ADAM-9 and ADAM-10. *J Comput Aided Mol Des* **17**, 551–565.